Optical scattering properties of soft tissue: a discrete particle model

Joseph M. Schmitt and Gitesh Kumar

We introduce a micro-optical model of soft biological tissue that permits numerical computation of the absolute magnitudes of its scattering coefficients. A key assumption of the model is that the refractive-index variations caused by microscopic tissue elements can be treated as particles with sizes distributed according to a skewed log-normal distribution function. In the limit of an infinitely large variance in the particle size, this function has the same power-law dependence as the volume fractions of the subunits of an ideal fractal object. To compute a complete set of optical coefficients of a prototypical soft tissue (single-scattering coefficient, transport scattering coefficient, backscattering coefficient, phase function, and asymmetry parameter), we apply Mie theory to a volume of spheres with sizes distributed according to the theoretical distribution. A packing factor is included in the calculation of the optical cross sections to account for correlated scattering among tightly packed particles. The results suggest that the skewed log-normal distribution function, with a shape specified by a limiting fractal dimension of 3.7, is a valid approximation of the size distribution of scatterers in tissue. In the wavelength range $600 \leq \lambda \leq 1400$ nm, the diameters of the scatterers that contribute most to backscattering were found to be significantly smaller ($\lambda/4$–$\lambda/2$) than the diameters of the scatterers that cause the greatest extinction of forward-scattered light (3–4λ).

OCIS codes: 170.6930, 350.4990, 290.0290.

1. Introduction

A growing number of applications of optical imaging and spectroscopy in medicine rely on measurement of the elastic scattering properties of tissue to detect underlying pathology.[1–4] Although it is recognized that the optical properties of tissue are related to its microstructure and refractive index, the nature of the relationship is still poorly understood. Previous investigations have focused on various aspects of this relationship, including the contribution of mitochondria to the scattering properties of the liver,[5] the spatial variations in the refractive index of cells and tissue sections,[6–8] and the diffraction properties of single cells.[9,10] Still lacking, however, is a quantitative model that relates the microscopic properties of cells and other tissue elements to the scattering coefficients of bulk tissue. Ideally, such a model should be able to predict the absolute magnitudes of the optical scattering coefficients as well as their wavelength and angle dependencies. Moreover, to assist in future efforts to invert measured data, the model should give insight into how the scattering properties are influenced by the numbers, sizes, and arrangement of the tissue elements.

This paper presents a framework for a particulate model of soft tissue that satisfies at least a few of these requirements. We identify the major elements in soft tissue responsible for the microscopic variations in its refractive index and, to facilitate numerical computations, treat the variations as discrete particles with statistically equivalent refractive indices. A skewed form of the log-normal distribution function is introduced to represent the size distribution of the particles. In the limit of an infinitely large variance in the particle size, this distribution function describes the volume fractions of the subunits of an ideal fractal object. Using Mie theory applied to a volume of spheres with diameters distributed according to the theoretical distribution, we calculate the wavelength dependence of the single-scattering coefficient, the transport-corrected scattering coefficient, and the asymmetry parameter of a tissue model. In addition to these more common op-

Joseph M. Schmitt is with the Department of Electrical and Electronic Engineering, Hong Kong University of Science and Technology, Clear Water Bay, Kowloon, Hong Kong. Gitesh Kumar is with the Perkin-Elmer Corporation, 50 Danbury Road, Wilton, Connecticut 06897-0208.

Received 18 August 1997; revised manuscript received 2 December 1997.

0003-6935/98/132788-10$15.00/0

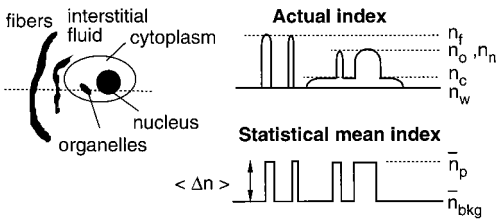

Fig. 1. Spatial variations of the refractive index of a soft biological tissue. A hypothetical index profile through several tissue elements is shown along with the profile through a statistically equivalent volume of homogeneous particles. The indices of refraction labeling the profiles are defined in Subsection 2.A.

tical constants, the phase function and backscattering coefficient are also calculated to study the influence of the microscopic composition of tissue on its angular scattering properties. Finally, we evaluate a complete set of optical coefficients of soft tissues containing different proportions of connective tissue fibers and make general observations about the sizes of scatterers in tissue responsible for attenuation and backscattering of a propagating light beam. The results suggest that the skewed lognormal distribution function, with a shape specified by the limiting fractal dimension, is a valid approximation of the distribution of sizes of scatterers in tissue.

2. Theory

Soft tissue is composed of tightly packed groups of cells entrapped in a network of fibers through which water percolates. Viewed on a microscopic scale, the constituents of the tissue have no clear boundaries. They appear to merge into a continuous structure distinguished optically only by spatial variations in the refractive index. To model such a complicated structure as a collection of particles, it is necessary to resort to a statistical approach.

A. Refraction-Index Variations: Particle Approximation

The results of earlier studies suggest that the tissue elements that contribute most to the local refractive-index variations are the connective tissue fibers (bundles of elastin and collagen), cytoplasmic organelles (e.g., mitochondria), and cell nuclei.[7] Figure 1 is a hypothetical index profile formed by measuring the refractive indices along a line in an arbitrary direction through a volume of tissue composed of these elements. The widths of the peaks in the index profile are proportional to the diameters of the elements, and their heights depend on the refractive index of each element relative to that of its immediate environment. Our goal here is to model the origin of the index variations by a statistically equivalent volume of discrete particles having the same index but different sizes. The index profiles in Fig. 1 illustrate the nature of the approximation implied by this model.

We first define the average background index as the weighted average of refractive indices of the cytoplasm and the interstitial fluid, n_c and n_s, as

$$\bar{n}_{\mathrm{bkg}} = f_c n_c + (1 - f_c) n_s, \tag{1}$$

where f_c is the fraction of the fluid in the tissue contained inside the cells. Estimated from the dissolved fractions of proteins and carbohydrates in the intracellular and interstitial fluids, n_c and n_s are approximately 1.36 and 1.34, respectively.[9] Since approximately 60% of the total fluid in soft tissue is contained in the intracellular compartment, it follows from Eq. (1) that $\bar{n}_{\mathrm{bkg}} = 0.4(1.34) + 0.6(1.36) = 1.352$. Next we define the refractive index of a particle as the sum of the background index and the mean index variation,

$$\bar{n}_p = \bar{n}_{\mathrm{bkg}} + \langle \Delta n \rangle, \tag{2}$$

which can be approximated by another volume-weighted average,

$$\langle \Delta n \rangle = f_f(n_f - n_s) + f_n(n_n - n_c) + f_0(n_0 - n_c). \tag{3}$$

Here subscripts f, n, and o refer to the fibers, nuclei, and organelles, which were identified above as the major contributors to index variations. The terms in parentheses in this expression are the differences between the refractive indices of the three types of tissue element and their respective backgrounds; the multiplying factors are the volume fractions of the elements in the solid portion of the tissue. The refractive index of the connective-tissue fibers is about 1.47, which corresponds to 55% hydration of collagen, its main component.[11] The nucleus and the cytoplasmic organelles in mammalian cells that contain similar concentrations of proteins and nucleic acids, such as mitochondria and the ribosomes, have refractive indices that lie within a relatively narrow range (1.39–1.42).[12,13] However, other cytoplasmic inclusions, particularly pigment granules, can have much higher refractive indices.[9] In this study we assumed $n_n = n_0 = 1.40$ so that f_n and f_0 need not be distinguished and Eq. (3) can be written in a simpler form as

$$\langle \Delta n \rangle = f_f(n_f - n_s) + (1 - f_f)(n_n - n_c). \tag{4}$$

This equation expresses the mean index variation in terms of the fibrous-tissue fraction f_f alone. Collagen and elastin fibers comprise approximately 70% of the fat-free dry weight of the dermis,[14] 45% of the heart,[15] and 2–3% of the nonmuscular internal organs.[16] Therefore, depending on tissue type, f_f may be as small as ~0.02 or as large as 0.7. For $n_f - n_s = 1.47 - 1.34 = 0.13$ and $n_n - n_c = n_o - n_c = 1.40 - 1.36 = 0.04$, the mean index variations that correspond to these two extremes are, according to Eq. (4), $\langle \Delta n \rangle = 0.02(0.13) + (1 - 0.02)(0.04) = 0.042$ and $\langle \Delta n \rangle = 0.7(0.13) + (1 - 0.7)(0.04) = 0.10$. Therefore these calculations suggest that the mean amplitude of the index variations in soft tissue lies between 0.04 and 0.10.

B. Particle Size Distribution

Having defined the refractive indices of the scattering particles, we are left with the task of determining their size distribution. The scattering centers in biological tissue span a wide range of dimensions and tend to aggregate into complex forms suggestive of fractal objects.[17,18] Recently, the fractal properties of tissue have been modeled by a distribution of particles whose number densities vary according to a power law.[6,19] Although a power-law distribution is the appropriate description of an ideal fractal object, the density functions of real objects rarely fit the same power law over more than a couple of decades.[20] In this study, we chose to employ a skewed logarithmic function to represent the distribution of sizes of particles in tissue. This function is more plausible on physical grounds, yet retains the essential character of the fractal description.

Written in its generalized form, the skewed logarithmic distribution function is[21]

$$f(x) = C_m x^m \exp\left[-\frac{(\ln x - \ln x_m)^2}{2\sigma_m{}^2}\right], \tag{5}$$

where x is the distributed variable (which can be chosen to be the diameter, area, or volume of particles), C_m is a normalizing factor, and the quantities x_m and σ_m set the center and width of the distribution, respectively. For $m = -1$ and $m = 0$, respectively, Eq. (5) is called the logarithmic normal distribution and zeroth-order logarithmic distribution, respectively.[21] Both distributions are used extensively in particle-size analysis. Here we treat $f(x)$ as the volume fraction of particles of diameter d and rewrite Eq. (5) in terms of a new set of variables:

$$\eta(d) = \frac{F_v}{C_m} d^{3-D_f} \exp\left[-\frac{(\ln d - \ln d_m)^2}{2\sigma_m{}^2}\right], \tag{6}$$

with

$$C_m = \sigma_m \sqrt{2\pi}\, d_m{}^{4-D_f} \exp[(4 - D_f)^2 \sigma_m^2/2],$$

where $\eta(d)$ is the volume fraction of particles with a diameter d and F_v is the total volume fraction of the particles, given by

$$F_v = \int_0^\infty \eta(d)\mathrm{d}d. \tag{7}$$

To establish a connection between the ideal fractal distribution used in previous studies,[6,7,19] we have written the exponent in Eq. (6) in terms of the (volumetric) fractal dimension D_f. Expressed in this way, the distribution takes on increasingly scale-invariant, or fractal, characteristics as its broadens. The parameter σ_m sets the fractal range over which the log–log slope of the distribution is approximately constant. In the limit of an infinitely broad distribution of particle sizes,

$$\lim_{\sigma_m \to \infty} \eta(d) \approx d^{3-D_f}. \tag{8}$$

For $3 < D_f < 4$, this power-law relationship describes the dependence of the volume fractions of the subunits of an ideal mass fractal on their diameter d.[22] For D_f equal to 3 (the Euclidean volume dimension), Eq. (6) reduces to the logarithmic normal distribution given by Eq. (5), with $m = -1$.

C. Optical Coefficients.

If it is assumed that the waves scattered by the individual particles in a thin slice of the modeled tissue volume add randomly, then the scattering coefficient of the volume can be approximated as the sum of the scattering coefficients of the particles of a given diameter,

$$\mu_s = \sum_{i=1}^{M} \mu_s(d_i), \tag{9}$$

where

$$\mu_s(d_i) = \frac{\eta(d_i)}{v_i}\, \sigma(d_i)$$

and M is the number of particle diameters; $\sigma_s(d_i)$ is the optical cross section of an individual particle with diameter d_i and volume v_i. The volume-averaged phase function of the tissue slice is the sum of the angular-scattering functions of the individual particles weighted by the product of their respective scattering coefficients,

$$P(\theta) = \frac{\sum_{i=1}^{M} \mu_s(d_i) P_i(\theta)}{\sum_{i=1}^{M} \mu_s(d_i)}. \tag{10}$$

Similarly, the asymmetry parameter, a measure of the anisotropy of light scattering within the tissue, is given by

$$g = \frac{\sum_{i=1}^{M} \mu_s(d_i) g_i(d_i)}{\sum_{i=1}^{M} \mu_s(d_i)}, \tag{11}$$

where

$$g_i(d_i) = \int_{-1}^{1} \cos\theta P_i(\cos\theta) d(\cos\theta)$$

is the mean cosine of the scattering angle of an individual particle of diameter d_i. The transport-corrected scattering coefficient, which is used extensively to model optical diffusion in thick tissues, is defined in terms of the asymmetry parameter as $\mu_{st} = \mu_s(1 - g)$. The volume-averaged backscattering coefficient, a variable used in earlier studies to characterize the reflectivity of microscopic samples,[23] is defined here as the sum of the particle cross sections

weighted by their angular-scattering functions evaluated at 180°,

$$\mu_b = \sum_{i=1}^{M} \frac{\eta(d_i)}{v_i}\, \sigma_s(d_i) P_i(180°). \tag{12}$$

Expressed in this manner, μ_b has units of $\mathrm{mm}^{-1}/\mathrm{sr}$, so that the product of μ_b and the thickness of the tissue slice yield the fraction of the incident irradiance backscattered per unit solid angle in the direction opposite to the incident light.

D. Correlated Scattering

In the calculation of the total scattering concentration of a mixture of particles, the usual assumption is that the particles scatter independently. However, because correlated scattering is likely in fractal media to be characterized by a high concentration of small particles, this assumption may be violated in tissues characterized by a high fractal dimension. Correlated scattering among particles with volume fractions higher than ~1% has been found to reduce the total scattering cross section when the diameters of the particles are much less than a wavelength.[24] In contrast, correlated scattering has been found to be insignificant among particles with diameters larger than a wavelength for volume fractions below ~10%.[24] To account for interparticle correlation effects, Twersky[25] derived an expression for the packing factor of a medium filled with a volume fraction h of subwavelength-diameter spheres:

$$W_s = \frac{(1-h)^4}{(1+2h)^2}. \tag{13}$$

W_s can be regarded as the fraction by which the bulk optical cross section diminishes as a result of correlated scattering among the spheres. Recently, Bascom and Cobbold[26] modified Eq. (13) to account for packing in a medium composed of scatterers with different shapes. Their modified packing fraction is

$$W_p = \frac{(1-h)^{p+1}}{[1+h(p-1)]^{p-1}}, \tag{14}$$

where p is a packing dimension that describes the rate at which the empty space between scatterers diminishes as the total number density increases. Although related, the packing and the fractal dimensions need not be the same. Packing of spherical particles is described well by a packing dimension $p = 3$, in which case Eq. (14) reduces to Eq. (13). On the other hand, the packing of sheetlike and rod-shaped particles is characterized by packing dimensions that approach 1 and 2, respectively. The elements of tissue have all of these different shapes and may exhibit cylindrical and spherical symmetry simultaneously. For a medium of this type, the packing dimension may lie anywhere between 1 and 5.[26] Adopting Eq. (14) as a general description of the packing fraction, we approximate the effective volume fraction of scatterers with the same diameter d as

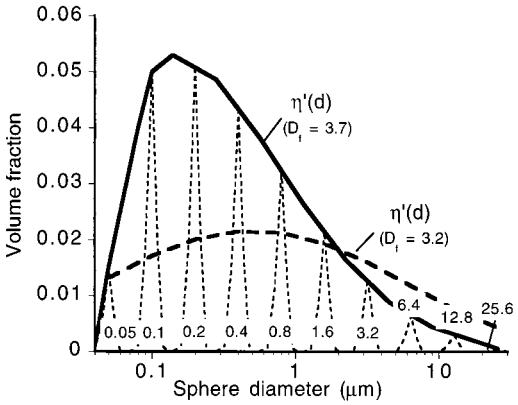

Fig. 2. Distribution of the volume fractions of spheres to which Mie theory was applied to calculate the scattering properties of tissue. Solid and dashed curves are the continuous correlation-corrected distributions given by Eq. (15) for $D_f = 3.7$ and $D_f = 3.2$. Dotted curves are the distributions of spheres with diameters increasing in powers of two from 50 nm to 25.6 μm that represent the $D_f = 3.7$ distribution. The partial volume fractions of the spheres were adjusted to conform to $\eta'(d)$, with their total volume fraction equal to F_v.

$$\eta'(d) = W_p \eta(d) = \frac{(1-\eta(d))^{p+1}}{[1+\eta(d)(p-1)]^{p-1}}\, \eta(d). \tag{15}$$

When we calculate the optical coefficients using Eqs. (9)–(12), the correlation-corrected distribution $\eta'(d)$ replaces $\eta(d)$.

3. Numerical Evaluation of Optical Properties

The expressions developed in Subsection 2.C were evaluated numerically to determine whether the model yields credible estimates of the phase function and the optical coefficients of tissue. Because of the wide range of particle diameters over which the summations in Eqs. (9)–(12) had to be evaluated, it was not practical to employ conventional discretized integration techniques. Instead, we used ten mean sphere diameters ranging from 50 nm to 25.6 μm in powers of two to represent the particles in the tissue model and their distributions. A Gaussian distribution (FWHM = $0.1d_i$) of sphere sizes centered on the mean diameters d_i was used to reduce the interference structure of the individual spheres. Figure 2 illustrates the shape of the continuous distributions for two values of D_f (3.7 and 3.2) and the method by which the distributions were approximated by the ten-sphere diameters. We chose to use spheres because this shape is consistent with the statistically isotropic nature of the refractive-index model and permits the application of Mie theory for calculation of the optical coefficients. However, it should be recognized that tissues that contain aligned fiber layers are not represented well by an isotropic model because their optical properties depend on the direction in which they are measured.

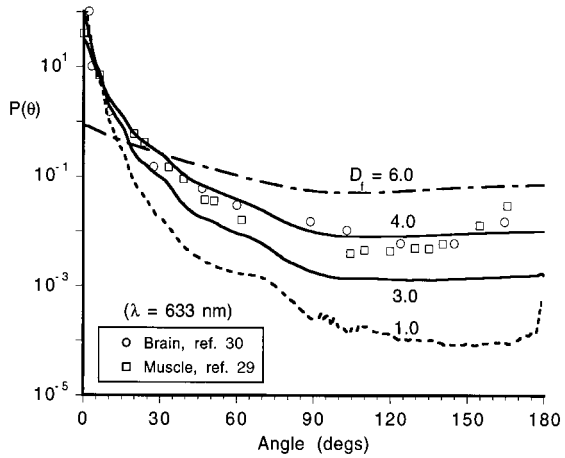

Fig. 3. Angular-scattering functions calculated with the ten-sphere tissue model for $D_f = 1, 3, 4$, and 6. Measurements of the angular scattering functions of muscle and brain that were taken from published studies are shown for comparison. Model parameters: $\bar{n}_{bkg} = 1.352$, $\bar{n}_p = 1.42$, $F_v = 0.2$, $d_m = 1.13$, $\sigma_m = 2$, $p = 3$.

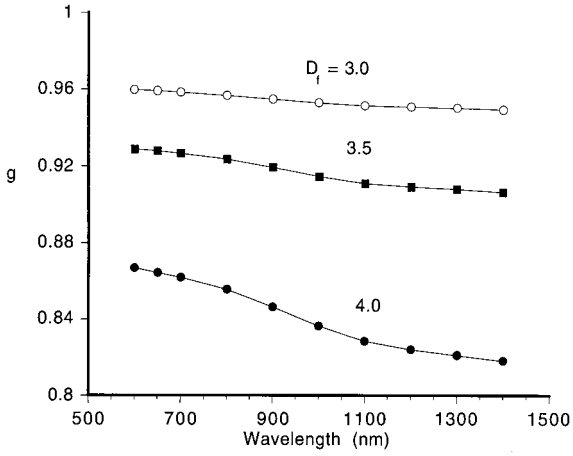

Fig. 4. Magnitude and wavelength dependence of the asymmetry parameter of a model tissue for values of the limiting fractal dimension D_f between 3 and 4. The dependence is weakest for low values of D_f because large particles contribute more to the total cross section. Model parameters: $\bar{n}_{bkg} = 1.352$, $\bar{n}_p = 1.42$, $F_v = 0.2$, $d_m = 1.13$, $\sigma_m = 2$, $p = 3$.

For most of the simulations, the refractive indices of the spheres and background medium were set equal to 1.42 and 1.352, respectively, to model a tissue with a refractive-index variation in the middle of the range calculated in Subsection 2.A. We adjusted the volume fractions of the spheres to scale according to the skewed logarithmic distribution [Eq. (6)]. The total volume fraction occupied by the spheres was estimated as $F_v = 1 - F_w - F_{pp}$, where F_w is the weight fraction of water in the tissue and F_{pp} is the fraction of organic solids in the combined interstitial fluid and cytoplasmic spaces. We chose $F_w = 0.75$ and $F_{pp} = 0.05$ as representative of human soft tissue[27] and set $F_v = 0.2$ to obtain the results given below in Section 4. The width parameter σ_m was fixed at 2.0 to match the fractal scaling range observed in earlier experiments (about one decade),[6] with d_m set equal to the geometric mean of the minimum and maximum sphere diameters in micrometers, $d_m = [(0.05)(25.5)]^{1/2} = 1.13$. The correlation-corrected distribution [Eq. (15)] with $p = 3$, the packing dimension for spheres, was applied in the numerical calculations of the cross sections. To compute the bulk optical coefficients of the modeled tissue, we evaluated the optical cross sections in Eqs. (9)–(12) in Subsection 2.C numerically, using a Mie-scattering algorithm (adapted from Ref. 28).

4. Results and Discussion

A. Angular Scattering Function

Angular scattering functions of a typical soft tissue represented by the ten-sphere numerical model are plotted in Fig. 3. The magnitudes are plotted without normalization for a range of fractal dimensions at a fixed wavelength ($\lambda = 633$ nm). For comparison, the angular-scattering functions of brain and muscle measured experimentally by Flock *et al.*[29] and Van der Zee *et al.*[30] are shown in the same figure. With the magnitude of the ratio between the indices of the particles and background fixed, the shape of $P(\theta)$ at a given wavelength is determined primarily by D_f. As D_f increases, the contribution of smaller particles increases, leading to a shift in the scattered power from the forward to the backward hemisphere.

Our results substantiate the observation of Gélébart *et al.*[19] that the phase function of a volume of spheres with a narrow distribution of diameters is a poor representation of the phase function of tissue. A wide range of sizes of scatterers must be used in the model to fit the shape of experimentally measured phase functions. For D_f in the range 3.5–3.9, the shape of $P(\theta)$ matches that of the phase functions of the brain and muscle well (Fig. 3). The only major discrepancy appears at angles close to the exact backscattering direction ($\theta = 180°$). At these angles, the amplitude of measured phase functions increases sharply, whereas the model curves remain almost flat. This sharp increase may be caused by the glory,[31] a phenomenon associated with very-large-size scatterers (>100 μm) not included in our numerical model, or it may be an experimental artifact caused by incompletely suppressed reflections at the surface of the tissue specimen. The similarity in the shapes of the experimental and the theoretical curves throughout most of the angular range supports the supposition that particle sizes in tissue are distributed like a fractal with a dimension in the range $3 < D_f < 4$. Values of D_f far outside of the fractal range give unrealistically flat or peaked phase functions characteristic of monodisperse distributions of Rayleigh or Mie scatterers (see curves $D_f = 6$ and $D_f = 1$ in Fig. 3).

B. Asymmetry Parameter

Figure 4 shows the computed magnitudes of the

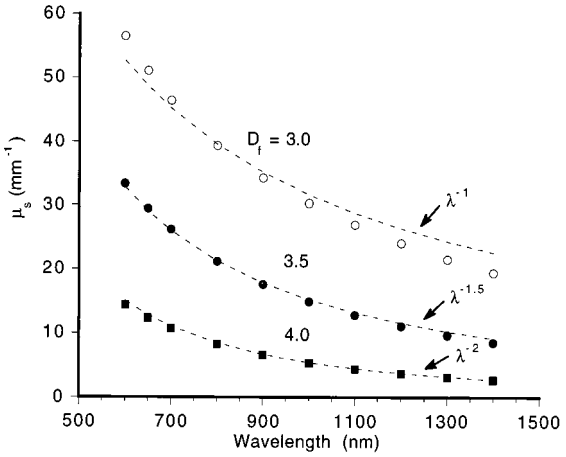

Fig. 5. Magnitude and wavelength dependence of the scattering coefficient μ_s of a model tissue for values of the limiting fractal dimension D_f between 3 and 4. Dashed curves are plots of the power-law function $\mu_s \approx \lambda^{2-D_f}$ versus wavelength. Notice the good fit of the curves for $D_f = 3.5$ and $D_f = 4.0$. Model parameters: $\bar{n}_{\mathrm{bkg}} = 1.352$, $\bar{n}_p = 1.42$, $F_v = 0.2$, $d_m = 1.13$, $\sigma_m = 2$, $p = 3$.

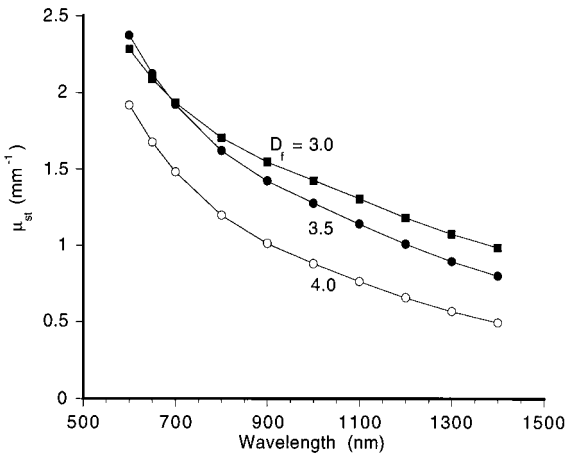

Fig. 6. Magnitude and wavelength dependence of the scattering coefficient μ_{st} of a model tissue for values of the limiting fractal dimension D_f between 3 and 4. The dependence of μ_{st} on wavelength is weaker compared with that of μ_s (see Fig. 5), and its log–log slope does not have a simple dependence on D_f. Model parameters: $\bar{n}_{\mathrm{bkg}} = 1.352$, $\bar{n}_p = 1.42$, $F_v = 0.2$, $d_m = 1.13$, $\sigma_m = 2$, $p = 3$.

asymmetry parameter g over the range of wavelengths between 600 and 1300 nm. The magnitude of g of the model tissue is nearly independent of wavelength for $D_f = 3$ and has a weak dependence on wavelength for the higher values of D_f shown. Most of the experimental measurements of g that have been made on biological tissues indicate that g exceeds 0.9 in the visible and near-infrared spectral regions.[32] Our model predicts $g > 0.9$ in these spectral regions for fractal dimensions below approximately 3.7.

C. Scattering Coefficients

The scattering coefficients predicted by the tissue model are plotted in Fig. 5 as a function of wavelength for three different values of D_f between 3 and 4. As expected, the magnitude of μ_s increases as the fractal dimension decreases because the larger particles, which have the largest optical cross sections, contribute relatively more to the total optical cross section of the tissue. Our results show that fixing the total volume fraction of particles and their refractive indices places upper and lower bounds on the magnitude of the scattering coefficient. The model predicts that a tissue consisting of a narrow distribution of large particles (modeled by choosing small values for D_f and σ_m, and a large value for d_m) would have the highest value of μ_s in the visible spectral range; a medium containing a narrow distribution of particles sizes with its mean skewed toward small diameters (D_f, σ_m large, and d_m small) would have the lowest value.

We observed that the scaling law for particle sizes used in the model results in a remarkably simple dependence of the total scattering coefficient on the wavelength: $\mu_s \sim \lambda^{2-D_f}$. The exponent of this power law is one less than the limiting fractal dimension of the volume-fraction distribution [Eq. (6)]. The fitted curves in Fig. 5 illustrate the accuracy of this approximation for different values of D_f. The deviation evident for $D_f = 3$ results from the correction for correlated scattering [Eq. (15)], which reduces the effective cross sections of the smallest diameter particles.

In contrast to μ_s, the transport-corrected scattering coefficient, μ_{st}, has a relatively weak dependence on D_f. Figure 6 shows that the magnitude of μ_{st} predicted by the model is between 1 and 2 mm^{-1} throughout most of the visible and near-infrared range for $3 \leq D_f \leq 4$. The implication of this result is that μ_{st} is relatively insensitive to the shape of the distribution of particle sizes; its magnitude is determined, for the most part, by the total volume fraction and refractive indices of the particles. Although the μ_{st}-versus-λ curves are fitted well by power-law curves, the log–log slope of the curves does not appear to have a simple relationship with D_f.

The magnitude and the wavelength dependence of μ_b are shown in Fig. 7. Like μ_{st}, μ_b has a weak dependence on D_f. However, in contrast to the smooth decline in the magnitude of μ_{st} wavelength, μ_b has a nonmonotonic dependence, first declining steeply in the visible region and then leveling off to a nearly constant value in the near infrared. This behavior is a consequence of the strong wavelength dependence of the scattering cross section of the subwavelength particles that contribute most to the total backscattering coefficient (see discussion in Subsection 4.E).

D. Optical Properties of a Soft Tissue Model: Comparison with Measured Values

Table 1 summarizes the optical properties predicted by the model at three wavelengths (λ = 633, 800, and 1300 nm) for a soft tissue containing different dry-

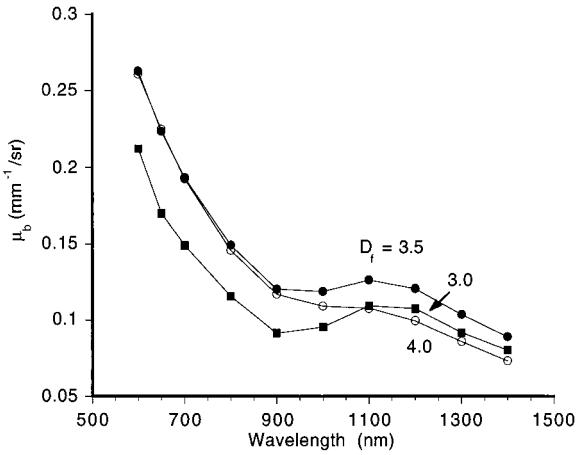

Fig. 7. Magnitude and wavelength dependence of the backscattering coefficient μ_b of the model tissue for values of the limiting fractal dimension D_f between 3 and 4. Model parameters: $\bar{n}_{bkg} = 1.352$, $\bar{n}_p = 1.42$, $F_v = 0.2$, $d_m = 1.13$, $\sigma_m = 2$, $p = 3$.

weight fractions of connective tissue fibers ($f_f = 0.03$, 0.3, and 0.7). The coefficients μ_s, μ_{st}, μ_b, and g in the table were computed for $D_f = 3.7$, the fractal dimension that yielded values that correspond best overall to available measurements. This value of D_f is also close to the fractal dimensions estimated by Fourier analysis of phase-contrast micrographs of fresh tissue sections in Ref. 6. (Note that the fractal dimensions given in this reference are given as area dimensions and therefore are one less than the volumetric dimensions used in this study.) Unfortunately, the accuracy of the predicted coefficients cannot be established at present because measurements of all four coefficients on living tissue are not available. However, measurements of the optical properties of excised tissue made by a number of researchers over the past decade have been compiled by Cheong *et al.*[32] Table 2 lists a set of coefficients selected from this compilation. The correspondence of these coefficients with the model results in Table 1 is discussed below.

The average value of μ_s measured at 633 nm on the different soft tissue types shown in Table 2 is 22 mm^{-1}, the same as the value that we found for the model tissue with $f_f = 0.3$, a proportion of connection tissue fibers about midway between the physiological extremes estimated in Subsection 2.A ($f_f = 0.02$ and $f_f = 0.7$). The strong dependence of the magnitude of the scattering coefficients on f_f underscores the sensitivity of scattering in tissue to the mean variation in the refractive index. In accordance with the model results, the measurements indicate that the magnitude of μ_s measured on the same tissue decreases substantially with wavelength. For example, Parsa *et al.*[33] measured a decrease in μ_s of rat liver from 14 mm^{-1} at 633 nm to 4.4 mm^{-1} at 1300

Table 1. Optical Coefficients of Model Tissues with Three Different Dry-Weight Fiber Fractions (f_f), for $D_f = 3.7$

	Wavelength (nm)								
	633			800			1300		
Coefficient	$f_f = 0.03$	$f_f = 0.3$	$f_f = 0.7$	$f_f = 0.03$	$f_f = 0.3$	$f_f = 0.7$	$f_f = 0.03$	$f_f = 0.3$	$f_f = 0.7$
μ_s (mm^{-1})	10.5	22.4	40.2	6.9	14.6	27.4	2.9	6.3	11.9
μ_{st} (mm^{-1})	0.80	2.0	4.5	0.57	1.4	3.2	0.30	0.75	1.65
μ_b (mm^{-1}/sr)	0.08	0.22	0.50	0.05	0.13	0.31	0.03	0.09	0.20
g	0.92	0.91	0.89	0.92	0.90	0.88	0.90	0.88	0.86

Table 2. Published Optical Properties of Tissues at Selected Wavelengths

Tissue Type	μ_s (mm^{-1})	μ_{st} (mm^{-1})	μ_b (mm^{-1}/sr)	g	Wavelength (nm)	Reference
Aorta (human)	31.6	4.1	—	0.87	633	Yoon *et al.*[35]
	17.1–31.0	2.6–3.7	—	0.81–0.91	633	Keijzer *et al.*[34]
	23.3	2.3	—	0.9	1320	Essenpreis[40]
Aorta (rat)	14.0–22.0	—	0.16 ± 0.1	—	800	Schmitt[38]
	11.0—20.0	—	0.05 ± 0.05	—	1300	Schmit[38]
Cartilage (human)	24.6	—	—	0.95	633	Qu *et al.*[36]
Liver (rabbit)	19.0	0.89	—	0.934	633	Beek *et al.*[39]
Liver (rat)	14.4	0.72	—	0.95	633	Parsa *et al.*[33]
	9.7	0.58	—	0.94	800	Parsa *et al.*[33]
	4.4	0.40	—	0.91	1300	Parsa *et al.*[33]
Myocardium (rabbit)	16.0–19.1	1.1	—	0.93–0.94	633	Beek *et al.*[39]
Skin, dermis (pig)	28.9	2.1	—	0.93	633	Beek *et al.*[39]
	25.4	1.4	—	0.95	790	Beek *et al.*[39]

nm. Their measured values of μ_s are close to those calculated for the model tissue with f_f between 0.03 and 0.3, and the calculated and measured scattering coefficients have nearly the same power-law dependencies on wavelength: $\mu_s \approx \lambda^{-1.7}$ (predicted) versus $\mu_s \approx \lambda^{-1.8}$ (measured).

The calculated value of g for the model tissue at 633 nm is approximately the same as the value measured for the aorta by Keijzer *et al.*[34] and Yoon *et al.*,[35] but the measured values of g in Table 2 are somewhat smaller for the rest of the tissues shown. The angular-scattering properties of tissues may reflect the relative contributions of the nuclei and the smaller organelles, such as the mitochondria.[9] The slow decline with wavelength in the magnitude of g predicted by the model is substantiated by the measurements of Parsa *et al.*[33] on rat liver (Table 2), but other investigators have found that g may also increase with wavelength.[36,37] The wavelength dependence of g is difficult to measure experimentally because the narrow forward-scattering peak of the phase function of tissue (see Fig. 3) makes averaging over angles prone to error.

The two measured values of μ_b listed in Table 2 were derived from the average magnitude of interference signals recorded in an earlier study by an optical-coherence microscope viewing an excised specimen of the aorta in the reflection mode.[38] The average backscattered powers, measured at $\lambda = 800$ nm and $\lambda = 1300$ nm relative to the incident powers, were found to equal -42 and -47 dB. Taking into account the thickness of the sample volume (20 μm) and the numerical aperture of the microscope (0.04), we calculated mean values of μ_b equal to 0.16 and 0.05 mm^{-1}/sr, respectively, at $\lambda = 800$ nm and $\lambda = 1300$ nm. These values agree fairly well with the backscattering coefficients of the model tissue calculated at the same wavelengths for $f_f = 0.3$ ($\mu_b = 0.13$ mm^{-1}/sr at $\lambda = 800$ nm and $\mu_b = 0.088$ mm^{-1}/sr at $\lambda = 1300$ nm). However, because of the interference noise in the measured signals, the precision of the measured values is poor. Additional studies need to be carried out to test the validity of the calculated backscattering coefficients.

E. Dominant Particle Sizes for Attenuation and Backscattering

An attractive feature of the tissue model is that it permits identification of the sizes of the particles in tissue that contribute most to attenuation and backscattering of light at a given wavelength. Figure 8 shows the contributions of each sphere size to the total scattering coefficient and backscattering coefficient in the ten-sphere model with $D_f = 3.7$ and $f_f = 0.3$. The widths of the distributions $\mu_b(d_i)$ and $\mu_s(d_i)$ indicate the wide range of particle sizes that are responsible for scattering in tissue. A convenient measure of the size of the particles that contribute most to extinction at a given wavelength is the centroid, $\langle d \rangle_{\text{ext}} = \Sigma_i\, d_i \mu_s(d_i) / \Sigma_i\, \mu_s(d_i)$; defined in a similar way, the centroid $\langle d \rangle_{\text{bk}} = \Sigma_i\, d_i \mu_b(d_i) / \Sigma_i\, \mu_b(d_i)$ is a convenient measure of the size of the particles that contribute most to backscattering. The calculated centroids of the distributions in Fig. 8 for $\lambda = 633$ nm are $\langle d \rangle_{\text{ext}} = 2.4$ μm and $\langle d \rangle_{\text{bk}} = 0.29$ μm. At the longer wavelength, $\lambda = 1300$ nm, the centroids shift toward larger values, $\langle d \rangle_{\text{ext}} = 4.0$ μm and $\langle d \rangle_{\text{bk}} = 0.38$ μm. From these results we conclude that the particles in tissues with diameters between $\lambda/4$ and $\lambda/2$ are the dominant backscatterers, whereas the particles that cause the greatest extinction of forward-scattered light have diameters between 3 and 4λ. An implication of this finding that pertains to optical-coherence microscopy and other thick-tissue imaging modalities is that large particles that attenuate a focused probe beam strongly may limit the penetration of the beam, yet backscatter too weakly to be seen. Conversely, small particles that backscatter strongly may cause little attenuation of a focused beam and therefore have a negligible effect on its penetration.

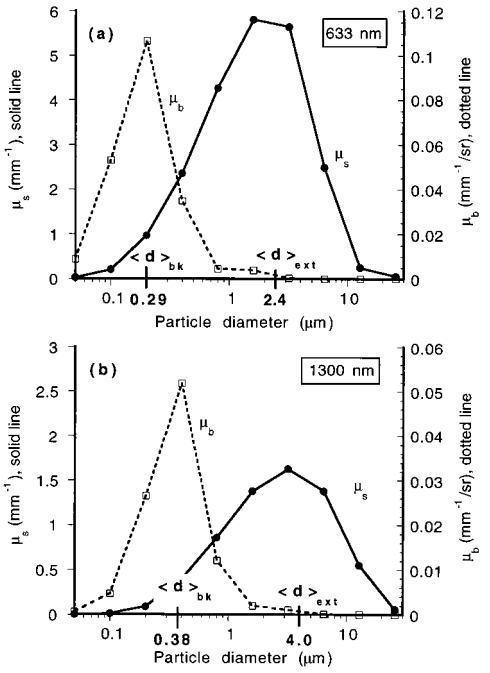

Fig. 8. Contributions of the different sizes of spheres in the ten-sphere model to the total scattering coefficient μ_s and backscattering coefficient μ_b of the model tissue for (a) $\lambda = 633$ nm and (b) $\lambda = 1300$ nm. The calculated values of the centroids of the distributions $\mu_s(d)$ and $\mu_b(d)$ are labeled on the x axes as $\langle d \rangle_{\text{ext}}$ and $\langle d \rangle_{\text{bk}}$, respectively. Model parameters: $D_f = 3.7$, $\bar{n}_{\text{bkg}} = 1.352$, $\bar{n}_p = 1.42$, $F_v = 0.2$, $d_m = 1.13$, $\sigma_m = 2$, $p = 3$.

5. Summary and Conclusions

In this study we have developed a micro-optical model that explains most of the observed scattering properties of soft biological tissue. The model treats the tissue as a collection of isotropic scattering particles whose volume fractions are distributed according to a skewed log-normal distribution [Eq. (6)] modified by a packing factor [Eq. (14)] to account for correlated scattering among densely packed particles. Ratios between the refractive indices of the

particles and background were derived from statistical arguments about the relative proportions of the microscopic elements of tissue and were found to range from 1.39/1.352 to 1.452/1.352, which correspond to dry-weight fractions of fibers between 0.03 and 0.3. After evaluating the model by applying Mie theory to a collection of spheres with a wide range of sizes, we found a set of parameters for the distribution and packing of the particles ($F_v = 0.2$, $D_f = 3.7$, $\sigma_m = 2$, $d_m = 1.13$, $p = 3$) that yields credible estimates of the scattering coefficients and asymmetry parameters of representative soft tissues. Applying this model, we observed the following: (1) as an optical medium, tissue is represented best by a volume of scatterers with a wide distribution of sizes, (2) fixing the total volume fraction of particles and their refractive indices places upper and lower bounds on the magnitude of the scattering coefficient, (3) the scattering coefficient decreases with wavelength approximately as $\mu_s \sim \lambda^{2-D_f}$ for $600 \leq \lambda \leq 1400$ nm, where D_f is the limiting fractal dimension, and (4) scatterers in tissue with diameters between $\lambda/4$ and $\lambda/2$ are the dominant backscatterers; the scatterers that cause the greatest extinction of forward-scattered light have diameters between 3λ and 4λ.

We hope that the model developed in this study will provide a starting point for further exploration of the micro-optics of tissue. Remaining problems include the influence of the arrangement of tissue elements on coherent optical scattering and the origins of the variability in the scattering coefficients of normal and pathological tissues.

References

1. M. S. Patterson, "Noninvasive measurements of tissue optical properties: current status and future prospects," Comments Mol. Cell. Biophys. A **8,** 387–417 (1995).
2. I. J. Bigio, J. R. Mourant, J. D. Boyer, T. M. Johnson, T. Shimada, and R. L. Conn, "Noninvasive identification of bladder cancer with subsurface backscattered light," in *Advances in Laser and Light Spectroscopy to Diagnose Cancer and Other Diseases*, R. R. Alfano, ed., Proc. SPIE **2135,** 26–35 (1994).
3. B. C. Wilson, E. M. Sevick, M. S. Patterson, and B. Chance, "Time-dependent optical spectroscopy and imaging for biomedical applications," Proc. IEEE **80,** 918–930 (1992).
4. G. Tearney, M. E. Brezinsky, B. E. Bouma, S. A. Boppart, C. Pitris, J. F. Southern, and J. G. Fujimoto," Science **276,** 2037–2039 (1997).
5. B. Beauvoit, T. Kitai, and B. Chance, "Contribution of the mitochondrial component to the optical properties of the rat liver: a theoretical and practical approach," Biophys. J. **67,** 2501–2510 (1994).
6. J. M. Schmitt and G. Kumar, "Turbulent nature of refractive-index variations in biological tissue," Opt. Lett. **21,** 1310–1312 (1996).
7. G. Kumar and J. M. Schmitt, "Micro-optical properties of tissue," in *Advances in Laser and Light Spectroscopy to Diagnose Cancer and Other Diseases III: Optical Biopsy*, R. R. Alfano and A. Katzir, eds., Proc. SPIE **2679,** 106–116 (1996).
8. J. Beuthan, O. Minet, J. Helfmann, M. Herrig, and G. Müller, "The spatial variation of the refractive index in biological cells," Phys. Med. Biol. **41,** 369–382 (1996).
9. A. Dunn and R. Richards-Kortum, "Three-dimensional computation of light scattering from cells," IEEE J. Sel. Top. Quantum Electron. **2,** 898–905 (1996).
10. B. Türke, G. Seger, M. Achatz, and W. van Seelen, "Fourier optical approach to the extraction of morphological parameters from the diffraction pattern of biological cells," Appl. Opt. **17,** 2754–2761 (1978).
11. V. Twersky, "Transparency of pair-correlated, random distributions of small scatterers, with applications to the cornea," J. Opt. Soc. Am. **65,** 524–530 (1975).
12. R. Barer, K. F. A. Ross, and S. Tkaczyk, "Refractometry of living cells," Nature (London) **171,** 720–724 (1953).
13. A. Brunsting and P. Mullaney, "Differential light scattering from spherical mammalian cells," Biophys. J. **14,** 439–453 (1974).
14. G. D. Weinstein and R. J. Boucek, "Collagen and elastin of human dermis," J. Invest. Dermatol. **35,** 227–229 (1960).
15. T. D. Scholz, S. R. Fleagle, T. L. Burns, and D. J. Skorton, "Nuclear magnetic resonance relaxometry of the normal heart: relationship between collagen content and relaxation times of the four chambers," Magn. Reson. Imag. **7,** 643–648 (1989).
16. M. Rojkind, M. A. Giambrone, and L. Biempica, "Collagen types in normal and cirrhotic liver," Gastroenterology **76,** 710 (1979).
17. B. J. West, "Physiology in fractal dimensions: error tolerance," Ann. Biomed. Eng. **18,** 135–149 (1990).
18. H. Honda, S. Imayama, and M. Tanemura, "A fractal-like structure in skin," Fractals **4,** 139–147 (1996).
19. B. Gélébart, E. Tinet, J.-M. Tualle, and S. Avrillier, "Phase function simulation in tissue phantoms: a fractal approach," Pure Appl. Opt. **5,** 377–388 (1996).
20. D. Hamburger, O. Biham, and D. Avnir, "Apparent fractality emerging from models of random distributions," Phys. Rev. E **53,** 3442–3458 (1996).
21. M. Kerker, *The Scattering of Light and other Electromagnetic Radiation* (Academic, San Diego, Calif., 1969), pp. 351–359.
22. B. B. Mandelbrot, *The Fractal Geometry of Nature* (Freeman, San Francisco, Calif., 1982), Chap. 12.
23. J. M. Schmitt, A. Knüttel, and R. F. Bonner, "Measurement of optical properties of biological tissues by low-coherence reflectometry," Appl. Opt. **32,** 6032–6042 (1993).
24. A. Ishimaru and Y. Kuga, "Attenuation constant of a coherent field in a dense distribution of particles," J. Opt. Soc. Am. **72,** 1317–1320 (1982).
25. V. Twersky, "Acoustic bulk parameters in distributions of pair-correlated scatterers," J. Acoust. Soc. Am. **64,** 1710–1719 (1978).
26. P. A. J. Bascom and R. S. C. Cobbold, "On the fractal packing approach for understanding ultrasonic backscattering from blood," J. Acoust. Soc. Am. **98,** 3040–3049 (1995).
27. F. A. Duck, *Physical Properties of Tissue* (Academic, New York, 1990), Chap. 9.
28. C. F. Bohren and D. R. Huffman, *Absorption and Scattering of Light by Small Particles* (Wiley, New York, 1983), Appendix A.
29. S. T. Flock, B. C. Wilson, and M. S. Patterson, "Total attenuation coefficients and scattering phase functions of tissues and phantom materials at 633 nanometers," Med. Phys. **14,** 835–841 (1987).
30. P. Van der Zee, M. Essenpreis, and D. T. Delpy, "Optical properties of brain tissue," in *Photon Migration and Imaging in Random Media and Tissues*, B. Chance and R. R. Alfano, eds., Proc. SPIE **1888,** 454–465 (1993).
31. V. Khare and H. M. Nussenzveig, "The theory of the glory," Phys. Rev. Lett. **38,** 1279–1282 (1977).
32. W. F. Cheong, "Summary of optical properties," in *Optical-Thermal Response of Laser-Irradiated Tissue*, A. J. Welch and M. J. C. van Gemert, eds. (Plenum, New York, 1995), pp. 275–303.
33. P. Parsa, S. L. Jacques, and N. S. Nishioka, "Optical properties of rat liver between 350 and 2200 nm," Appl. Opt. **28,** 2325–2330 (1989).

34. M. Keijzer, R. R. Richards-Kortum, S. L. Jacques, and M. S. Feld, "Fluorescence spectroscopy of turbid media: autofluorescence of the human aorta," Appl. Opt. **28,** 4286–4292 (1989).
35. G. Yoon, "Absorption and scattering of laser light in biological media—mathematical modeling and methods for determining optical properties," Ph.D. dissertation (University of Texas, Austin, Tex., 1988).
36. J. N. Qu, C. MacAulay, S. Lam, and B. Palcic, "Optical properties of normal and carcinomatous bronchial tissue," Appl. Opt. **33,** 7397–7405 (1994).
37. V. G. Peters, D. R. Wyman, M. S. Patterson, and G. L. Frank, "Optical properties of normal and diseased human breast tissues in the visible and near infrared," Phys. Med. Biol. **35,** 1317–1334 (1990).
38. J. M. Schmitt, A. Knüttel, M. Yadlowsky, and M. A. Eckhaus, "Optical-coherence tomography of a dense tissue: statistics of attenuation and backscattering," Phys. Med. Biol. **39,** 1705–1720 (1994).
39. J. F. Beek, H. J. van Staveren, P. Posthumus, H. J. C. M. Sterenborg, and M. J. C. van Gemert, "The influence of respiration on the optical properties of piglet lung at 632.8 nm," in *Medical Optical Tomography: Functional Imaging and Monitoring*, G. Müller, B. Chance, R. R. Alfano, S R. Arridge, J. Beuthan, E. Gratton, M. Kaschke, B. R. Masters, S. Svanberg, and P. van der Zee, eds. (SPIE Optical Engineering Press, Bellingham, Wash., 1993), Vol. IS11, pp. 193–210.
40. M. Essenpreis, *Thermally Induced Changes in Optical Properties of Biological Tissues* (University College London, England, 1992).

Applied Optics needs

Patent Reviewers

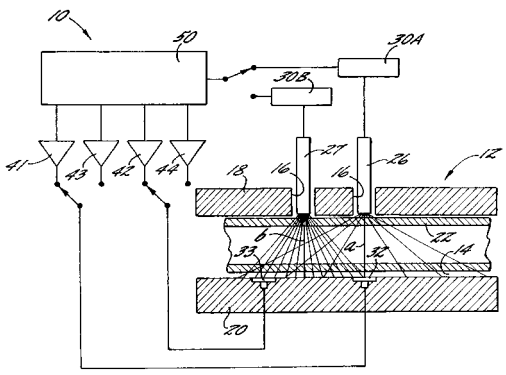

Members of the *Applied Optics* Patent Review Panel periodically choose or are sent new patents for review. Reviewers are unpaid volunteers. The reviewer writes a one-paragraph summary and review of the patent; he or she frequently chooses an illustration from the patent to appear with the review. Patent reviews are published in the appropriate division of *Applied Optics* as a sufficient number of reviews become available.

Applied Optics especially needs patent reviewers with expertise in all fields, but especially in the following areas:

Alignment	Biomedical Optics	Colorimetry
Information Processing	Thin Films	Graded-Fiber Optics
Graphics, Halftones	Modulators	Liquid Crystals
Lithography	Photometry	Monochromators
Ophthalmic Applications	X-Ray Optics	Phase conjugation

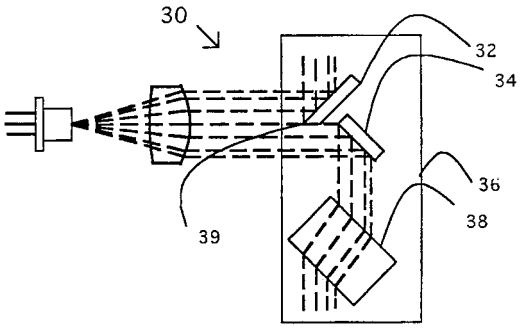

Applicants should please state whether they have Internet access.

Interested persons should send a brief curriculum vitae and bibliography, by post or by e-mail, to

Barbara Williams
Patent Reviewer Search
Optical Society of America
2010 Massachusetts Ave. NW
Washington, DC 20036-1023

bwilli@osa.org, subject “patent reviewer”

Manuscript Submission Form

TITLE: _____

_____

AUTHORS: _____

_____

CORRESPONDING AUTHOR: _____

ADDRESS: _____

_____

_____

TELEPHONE: _____ FAX: _____

E-MAIL: _____

Journal to which you are submitting your manuscript (check only one):

- ☐ J. Opt. Soc. Am. A: Optics & Image Science
- ☐ J. Opt. Soc. Am. B: Optical Physics
- ☐ Optics Letters
- ☐ Applied Optics: Optical Technology & Biomedical Optics
- ☐ Applied Optics: Information Processing
- ☐ Applied Optics: Lasers, Photonics, & Environmental Optics

☐ The author gives permission to transfer the manuscript to another OSA journal, without further correspondence, if the editor believes that such a transfer is appropriate.

☐ Optics Letters routinely faxes manuscripts to reviewers. If your manuscript contains figures that must be mailed to ensure readability, please check here.

To avoid unnecessary duplication of information in archival sources and to minimize costs to subscribers, the OSA seeks to limit multiple publication of the same scientific results. If a significant portion of the information in your manuscript has appeared in or has been submitted simultaneously to another publication, you are encouraged to aid the refereeing process by indicating, separately from the manuscript, the new content in the contribution now being submitted.

Authors are strongly urged to include a list of at least four individuals who may be appropriate reviewers for their manuscripts. These suggestions will be used at the topical editor's discretion, and should expedite the peer review process.

Potential reviewers (name, affiliation, telephone, fax, or e-mail.)

_____

_____

_____

_____

[over]

As an aid to the indexer, please list a maximum of six keywords using the Optics Classification and Indexing Scheme (**OCIS**) terms. The complete list of terms may be found on OpticsNet (www.osa.org). It is also published periodically in the OSA's journals. Free terms may also be used if an appropriate term is not found. If using a free term, use the code # 999.9999 and write in your term.

OCIS number	term	OCIS number	term

If a thorough review would require that referees read your related works that are currently submitted or in press, please enclose three copies of these papers.

Closely related works that you have published:
(enclose 3 copies if not yet published)

_____

_____

_____

Overlength Publication Charges

JOSA A and JOSA B require payment of an overlength publication charge of $210 per printed page in excess of ten. *Applied Optics* has an overlength publication charge of $105 per printed page in excess of eight. *Optics Letters* is limited to three journal pages and does not incur an overlength charge. To roughly estimate the length of your JOSA or *Applied Optics* paper, divide the number of double-spaced manuscript pages, including illustrations by four. Please check your manuscript for compliance with these limits.

Author Certifications

I certify that, to the best of my knowledge, this manuscript contains new content not previously published or submitted elsewhere for simultaneous consideration. I further certify that all authors have agreed to the submission of this manuscript to the OSA journal specified above.

I have checked the manuscript length. I agree to pay the overlength charges noted above if they are applicable to my paper.

The *OSA Copyright Transfer Agreement* form is enclosed.

_____ _____

Signature **Date**

Return this form to:
The Optical Society of America
ATTN: Manuscript Office
2010 Massachusetts Ave., N.W.
Washington, DC 20036-1023